National Research University Higher School of Economics

as a manuscript

Belikov Ivan Igorevich

Development of terahertz integrated devices with dielectric waveguides based on Si and GaAs

Dissertation summary
for the purpose of obtaining academic degree
Doctor of Philosophy in Engineering

Academic supervisor:
Doctor of Philosophy in Physical and Mathematical Sciences
Shurakov Alexander Sergeevich

Moscow — 2026

Introduction

Terahertz (THz) electronics has been the subject of a large number of scientific studies over the past few decades. Working with THz radiation provides benefits in medical systems, security systems, meteorological instruments, material science, and astronomical instruments. One of the promising areas is research in the field of radiophotonics and integrated photonics. In particular, the expediency of using THz photonic integrated circuits in new-generation communication systems to provide ultrafast generation and signal processing on a chip was demonstrated recently [1; 2]. For operating frequencies above 300 GHz, silicon integrated circuits (ICs) using photonic crystal waveguides and effictive dielectric media are in area of interest. Such photonic integrated circuits (PICs) can contain a large number of devices with various active and passive elements (concentrated, distributed or both). The use of PICs can reduce its own losses in the circuitry and increase the integration level of various nonlinear devices into the circuits. The usage of photonic power distribution lines not only reduces signal processing losses on the chip, but also helps to avoid numerous problems associated with the packaging and assembly of the devices. The synergy of electronic and photonic processing of THz signals is recognized as one of the most promising approaches [3; 4]. However, the development of nonlinear frequency conversion devices technologically compatible with the silicon platform is at an early stage. Different types of planar waveguides are usually used to provide a connection between the elements in an IC at frequencies above 1 THz. Despite the fact that the use of such waveguides makes it possible to create complex structures on a chip within a single IC, propagation losses remain high. Hollow metal waveguides are often used in THz waveguide circuits, however, propagation losses reach several dB/cm at a frequency of 1 THz, and their use requires precision mechanical assembly when implementing a modular architecture. Planar metal waveguides may be produced within the cleanroom technological processes, therefore they are used in monolithic integrated circuits, while propagation losses reach tens of dB/cm at a frequency of 1 THz. Dielectric waveguides are also manufactured

within the cleanroom technological processes and allow the implementation of power distribution lines on a chip and a feeder path for the input of optical radiation. Integrated circuits based on such waveguides do not require assembly, and propagation losses are fractions of dB/cm at a frequency of 1 THz, which makes it possible to obtain extreme sensitivities in devices for detecting and processing THz signals. The usage of dielectric waveguides is one of the most promising ways to implement THz PIC. Among the existing THz radiation detectors, superconducting hot electron bolometers (HEBs) are quite a distinguished group. HEB detectors are widely used as mixing elements in the composition of heterodyne receivers in radio astronomy tasks. To effectively solve the problems of modern radio astronomy using ground-based telescopes, it is necessary to master a new 7-14 THz frequency range for practical heterodyne receiving systems. Due to the frequency-independent response generation mechanism and the practical combination of sensitivity and speed due to the effect of electronic heating [5], the inclusion of HEB mixers in the composition of THz PIC is an urgent task. Radiophotonic and photonic integrated circuits of a lower frequency range of 0,1–0,3 THz may be in demand in modern image construction and wireless communication systems. Despite the fact that modern solid-state wireless modules typically use a silicon platform to generate and process THz signals [6; 7], the steady progress of microelectronic device manufacturing technologies makes it possible to complement classic silicon devices and systems with their A(III)B(V)-based counterparts, which can provide benefits in the THz range [8; 9]. One of the promising areas of application of terahertz ICs is beam steering devices for new generation communication networks in the carrier frequency range of 140-150 GHz. Effective beam management is required to create and maintain virtual line-of-sight channels, which is designed to prevent possible signal fading and connection failures. The use of terahertz spatial modulators is proposed as a solution to this problem [10]. These structures use either antenna arrays or metasurfaces [11; 12] with dielectric insulated metallization layers. Such solutions allow efficient wavefront processing including phase, amplitude or polarization modulation [13]. In the case

of static beam formation, the wavefront parameters can be changed by modifying the geometry of the cell of the reconfigurable surface [14]. Devices for semi-static and dynamic beam control use integrated tuning elements such as liquid crystals, microelectromechanical systems, phase memory materials, or ultrafast electronics based on transistors and diodes [15]. GaAs-based Schottky diodes are a promising device for integration as tuning elements in ultrafast electronic scanning systems. At the same time, their application requires a study of the effectiveness of integrating diodes into multi-element ICs and reducing parasitic characteristics.

Thus, the **relevance** of this dissertation research is due to the need to expand the element base of modern micro- and nanoelectronics in terms of integrated devices for spectral analysis and spatial modulation of signals in a new and actively developed spectral range – the terahertz range.

The purpose of this research work is to investigate the possibility of performing elements of photonic integrated circuits with superconducting NbN/Si hot electron bolometers and planar Ti/Pt/Au/n-GaAs Schottky diodes for spectral analysis and spatial modulation of signals in the terahertz range.

To achieve the set purpose, the following **tasks** were proposed:

1. To propose a design of a niobium nitride hot electron bolometer utilizing silicon waveguide structures (NbN/Si HEB) for photonic integrated circuits with extremely low propagation losses in the terahertz range.

2. To study the possibility of creating an PIC with HEB NbN/Si mixer, including input lines for heterodyne power and signal radiation, and signal capture at an intermediate frequency at operating frequencies above 2,5 THz.

3. To propose ways of reducing losses in a diode element based on the Ti/Pt/Au/n-GaAs Schottky microcontact using as part of a spatial signal modulator with a central operating frequency of 150 GHz.

4. To study the influence of the design and manufacturing processes of superconducting NbN/Si hot electron bolometers and planar Ti/Pt/Au/n-GaAs Schottky diodes on the electronic and radiophysical characteristics of terahertz photonic integrated circuits based on them. Formulate conclusions.

Elements of terahertz photonic integrated circuits with superconducting NbN/Si hot electron bolometers and planar Ti/Pt/Au/n-GaAs Schottky diodes were selected as the **Object** of the study.

The influence of the design and manufacturing method of superconducting NbN/Si hot electron bolometers and planar Ti/Pt/Au/n-GaAs Schottky diodes on the electronic and radiophysical characteristics of terahertz photonic integrated circuits based on them were selected as the **Subject** of the study.

Scientific novely of the research.

1. A new design of a niobium nitride hot electron bolometer utilizing silicon waveguide structures (NbN/Si HEB) for photonic integrated circuits with extremely low propagation losses in the terahertz range has been demonstrated.

2. The possibility of creating an PIC of NbN/Si HEB mixer, including input lines for heterodyne power and signal radiation, and signal capture at an intermediate frequency with a central operating frequency of 2,7 THz were demonstrated for the first time.

3. Technological terahertz PIC of antenna devices based on silicon and gallium arsenide substrates have been developed and studied.

4. Original methods of reducing losses in a diode element based on the Ti/Pt/Au/n-GaAs Schottky microcontact using as part of a spatial signal modulator with a central operating frequency of 150 GHz were proposed.

Practical relevance.

At frequencies above 2,5 THz, terahertz photonic integrated circuits and devices based on them are in demand in instrument complexes of modern radio astronomy

for spectral measurements of objects of galaxies with moderate resolution (10^2-10^3). The developed monolithic terahertz mixer based on high-resistance Si waveguide structures is the basic element for implementing a terahertz spectrometer on chip that meets these criteria. Radiophotonic and photonic integrated circuits of a lower frequency range of 0,1–0,3 THz are in demand in modern systems of image construction and wireless communication. The developed terahertz planar diode with a Schottky microcontact is the basic element for the implementation of a photonic integrated circuit of a spatial terahertz modulator with moderate energy consumption (up to 500 μW per cell) based on GaAs, designed to distribute a radio signal in reflected light. Constructions and methods of manufacturing elements of terahertz photonic integrated circuits with superconducting NbN/Si hot electron bolometers and planar Ti/Pt/Au/n-GaAs Schottky diodes, it is possible to expand the element of modern micro-nanoelectronics in terms of integrated devices for a new spectral range that is actively being developed in practical applications . The technical solutions obtained by the author for photonic integrated circuits with superconducting hot electron bolometers were used to improve the products of «Tirphotonics» LLC, which shows a successful **implementation result**. Technical solutions for photonic integrated circuits with planar Schottky diodes were patented in the form of a utility model (patent No. RU233164U1 dated 06/26/2024).

Methodology and research methods.

During the research, numerical calculation methods were used for solving the Maxwell system of equations to model the field pattern in the studied devices and their elements at the development stage; also analytical calculation and approximation of electronic characteristics using physical models of the studied devices at the stage of development and experimental research were used; methods of forming and processing materials using photo- and electron-beam lithography, thermal, electron beam and magnetron sputtering, liquid and plasma chemical etching for the manufacture of the studied devices. To analyse the geometric parameters of the manufactured devices, quality control methods based on optical, scanning electron (SEM) and

atomic force (AFM) microscopy were used. The electronic and radiophysical characteristics of the manufactured devices were studied using measurement methods for volt-ampere characteristics, scattering parameters, volt-watt sensitivity and noise equivalent power.

Provisions presented for defense:

1. Photonic integrated circuit of a superconducting NbN/Si HEB mixer with an operating frequency of 2,7 THz, including 8 dielectric rod antennas, 2 multimode interference-based power combiners, 1 photonic crystal waveguide with a distributed Bragg reflector and a mode converter based on a symmetrical silicon slotted line with a resistivity of 5-10 kOhm·cm and a thickness of 27 μm, at the end input, the radiation has a gain of 12,1 dBi with a side lobe level of -11 dB and internal losses for the input lines of a terahertz signal of 2,4-4,4 dB and a heterodyne power of 4,4-7,1 dB, a critical temperature of 9,3 K and a superconducting junction width of 1,6 K.

2. Terahertz planar Ti/Au/n-GaAs Schottky diode with three-level $n/n_+/n_{++}$-GaAs doping profile $4\times10^{17}/1\times10^{18}/5\times10^{18}$ cm^{-3} and a buffer layer thickness of n_+/n_{++} 0,86 μm has an ideality factor of 1,5, an average barrier height of 0,76 eV and a standard deviation of the barrier height of 0,12 eV with a Schottky contact size of 3 μm.

3. A terahertz planar Ti/Pt/Au/n-GaAs Schottky diode with an Γ-shaped suspended anode bridge, obtained from GaAs orientation (100) using an ammonia-based selective etchant, has a cutoff frequency of 13 THz, an ideality factor of 1,2, a barrier height of 0,8 eV, and a series resistance of 4 Ohm.

The degree of reliability of the obtained results.

The correspondence of the research results on a qualitative and quantitative level to the materials presented in scientific and technical works by other authors confirms the reliability and credibility of the final result.

Results were reported at 3 international and 3 all-Russian conferences to prove the scientific results. At the same time, 2 reports were presented orally and 4 were presented in poster format.

Publications.

17 scientific papers were published on the topic of the dissertation research. At the same time, 5 articles have been published in peer-reviewed journals that are included in the lists of recommended HSE journals; 8 articles have been published in publications included in the Scopus citation system and recommended by the Higher Attestation Commission; 4 papers are indexed by the RSCI.

The author's personal contribution to the research

The author took an active part in:

- Formulation of the topic, purpose setting and research tasks.
- Design and manufacturing of the devices under study.
- Experimental study of the electronic and radiophysical characteristics of the manufactured devices.
- Processing and analysis of data obtained as a result of experimental research.
- Presentation of research results at international and all-Russian conferences with oral and poster presentations.
- Preparation and publication of scientific articles in international peer-reviewed publications included in the lists of the Higher School of Economics (Lists A and C), Web of Science, Scopus, RSCI.

Contents

The dissertation consists of an introduction, a literature review, 2 chapters, a conclusion, a list of the author's publications and a bibliography. The total volume of the dissertation is 115 pages, of which 98 pages of text, including 54 figures and 9 tables. The bibliography includes 117 titles on 13 pages.

In the **introduction** the substantiation of the relevance of the topic, scientific novelty and practical significance of the thesis is formulated, the purpose and objectives are formulated, the scientific novelty of the research is shown, and the scientific positions submitted for defense are presented.

The **first chapter** presents an analytical review of the literature. The current level of development in the field of spectral measurement tools in terahertz astronomy, as well as spatial signal modulation devices for imaging systems and wireless communications, is described. The possibilities and prospects of using photonic integrated circuits based on semiconductor platforms of silicon and gallium arsenide in the lower and upper parts of the terahertz range - up to 0,3 THz and above 2,5 THz are analyzed.

In the **second chapter**, an original NbN HEB mixer design utilizing Si waveguide structures for the frequency range above 2,5 THz is proposed. The electromagnetic model and its verification by experiment are presented. The influence of manufacturing technology on the superconducting properties of a HEB device and an assessment of its manufacturability for inclusion in a photonic integrated circuit of a spectrometer on a chip in the 3-7 THz range are described. The main results were published by the author in [A1—A5]. The figure 1 shows a three-dimensional (3D) model of an almost completely dielectric HEB mixer with an operating frequency of 2,7 THz. The parameters of the hole grid in Si determine the geometry of photonic power distribution networks and photonic crystal waveguides. A four-contact electrical connection for direct current bias is also provided.

The basis of the proposed design is the conversion of an electromagnetic wave propagating in a dielectric medium into an alternating current in a superconducting sensing element. The conversion can be performed by attaching the HEB to a photonic crystal waveguide either directly or through a planar metal probe.

The figure 2 shows an effective transition from a single-mode flat silicon waveguide to an NbN microbridge with a resistance of 50 Ohm. The design was developed using iterative electromagnetic modeling in HFSS. In the framework of the simulation,

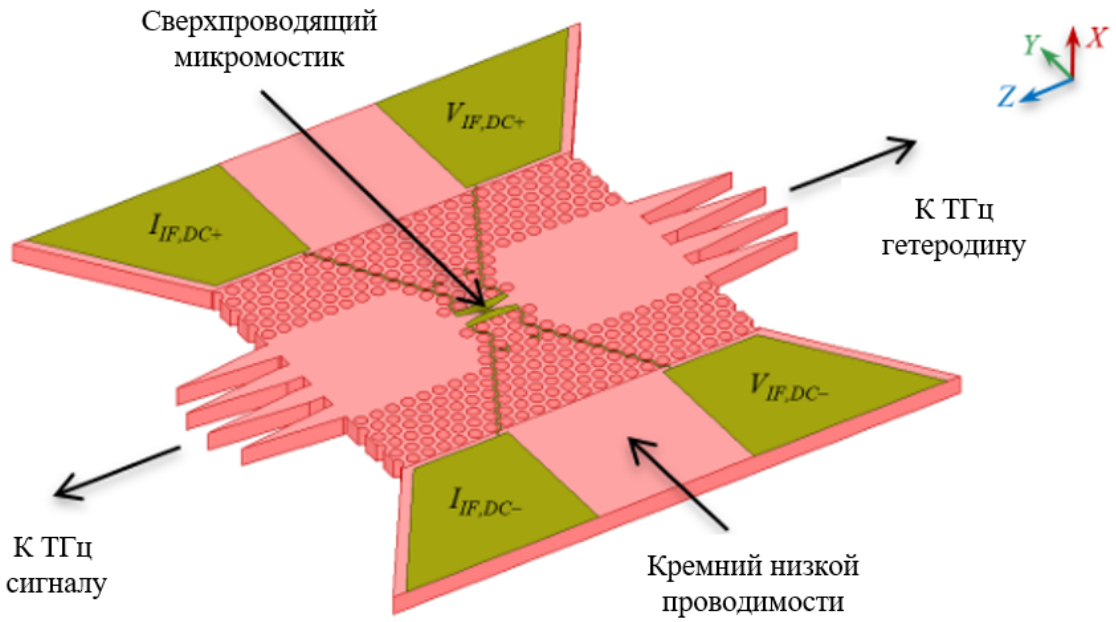

Fig. 1. 3D model of a THz HEB mixer with Si waveguide structures.

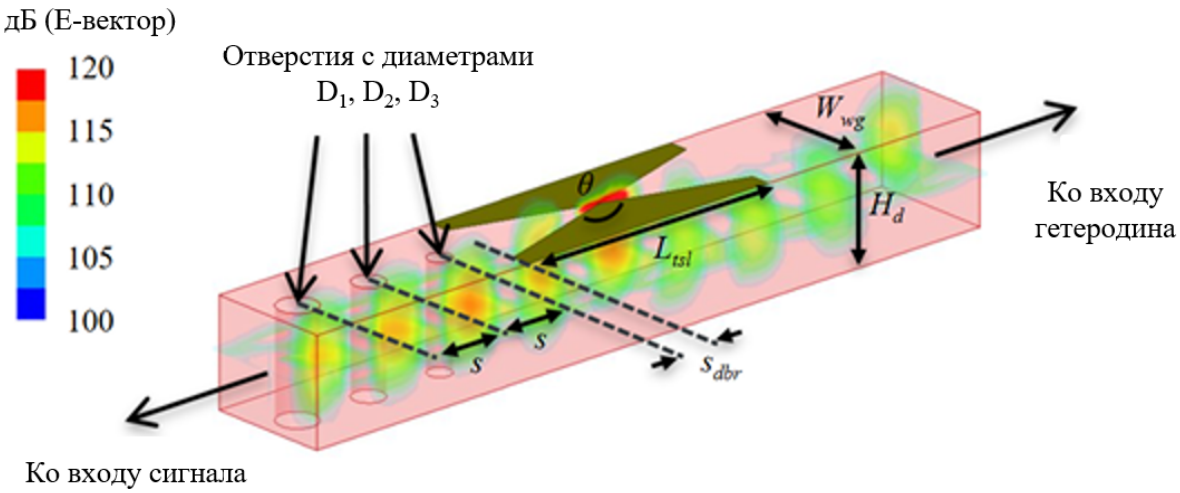

Fig. 2. Electromagnetic (EM) model of a segment of a flat silicon waveguide with a built-in slot line for a frequency of 2,7 THz.

dielectric losses in silicon were neglected, while its relative permittivity was assumed to be 11,9. The side walls of the waveguide are surrounded by quarter-wave vacuum inserts with an external boundary condition «Radiation». The front and rear ends of the waveguide are excited by two wave ports (ports 1 and 2). Communication between ports is controlled using a distributed Bragg reflector. The reflector is represented by three holes with a diameter of D_1, D_2, and D_3 in the waveguide at the input of the THz signal. A conical line with an integrated sensing element is

defined as a flat gold conductive structure with a point port in the center (port 3). The geometric parameters of the transition, designed to operate at a frequency of 2,7 THz, are shown in the table 1.

Table 1. Si geometry of a ribbon waveguide with an integrated slot line for operation at a frequency of 2,7 THz.

H_d, μm	W_{wg}, μm	L_{tsl}, μm	θ, $^\circ$	s_{dbr}, μm	s, μm	D_1, μm	D_2, μm	D_3, μm
27	32	70,9	146	11,9	21	10	8	6

Based on the simulation results, the scattering parameters $S33 = 16,1$ dB and $S31 = S32 = 4,4$ dB were obtained in the configuration without a reflector. With a Bragg reflector, $S33 = 32,3$ dB, $S31 = 2,4$ dB, and $S32 = 7,1$ dB. A further increase of $S31$ to about 1 dB is possible due to a sharp decrease in $S32$. This option becomes attractive, for example, if an incoherent detector is being designed and a heterodyne is not required. To increase the efficiency of radiation coupling between the signal and sensitive element of the mixer, transitions to free space in the form of fork antennas are formed at the beginning and end of the silicon waveguide. Each antenna is represented by a four-element array of rod antennas integrated with 4 ports of a multimode interference-based power combiner, as shown in the figure 3.

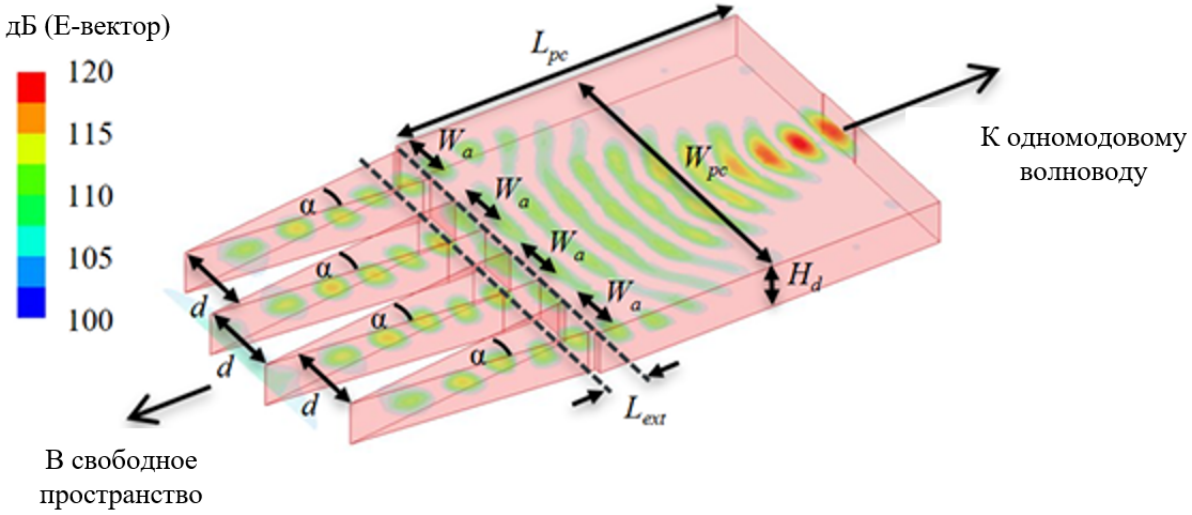

Fig. 3. An EM model of a rod antenna array integrated with a power combiner.

The processing of each supported m-th mode at the output of the rod antenna

array is carried out using a power combiner based on multimode interference with the corresponding phase constant, defined as:

$$\beta_m = \frac{2\pi\sqrt{\epsilon_r}}{\lambda_0} - \frac{\pi\lambda_0(m+1)^2}{4{W_{eff}}^2\sqrt{\epsilon_r}} \quad (1)$$

Here ϵ_r is the relative permittivity of the medium, λ_0 is the wavelength in free space, m is the number of modes, $W_{eff}(W_{pc}, L_{pc})$ is the effective width of the waveguide, depending on the length and width of the photonic crystal waveguide. The superposition of the assembled modes leads to four evenly distributed power maxima at the input of the combiner. A phase shift of almost 90° occurs in the side ports of the combiner relative to the central ports. To create a one-dimensional antenna array with uniform amplitude distribution and zero phase shift between the antennas, the two central antennas were extended using silicon inserts. Detailed information about the developed geometry for a frequency of 2,7 THz is given in the table 2.

Table 2. The geometry of the array of rod antennas integrated with a power combiner for a frequency of 2,7 THz.

H_d, μm	W_{pc}, μm	L_{pc}, μm	W_a, μm	L_{ext}, μm	α, °	d, μm
27	205,6	222,2	30,6	19,5	12	55,5

A hexagonal lattice with holes of $D = 18$ microns diameter and lattice constants of $A_Z = 23,4$ microns and $A_Y = 40,5$ microns is implemented on a silicon substrate with a thickness of 27 microns. Based on the lattice constraints, the width of the waveguide was assumed to be $W_{pc} = 194,1$ microns, and the length of the waveguide, in turn, $L_{pc} = 213,2$ microns. The analysis of the radiation pattern in the developed mixer design did not reveal an increase in losses at the power inputs of the heterodyne and the THz signal when combining its elements. As a result of the simulation after the introduction of the above changes, fork silicon antennas demonstrate a gain of 12,1 dB with a side lobe level of -11 dB. The beam width was 17° in the plane of

the mixer chip. To verify the calculation results, a sample of the antenna device of the developed design, a fork antenna, was made on a scale of 50:1 using mechanical processing of a dielectric substrate with a relative permittivity of 10,2 and a tangent loss of 0,003.

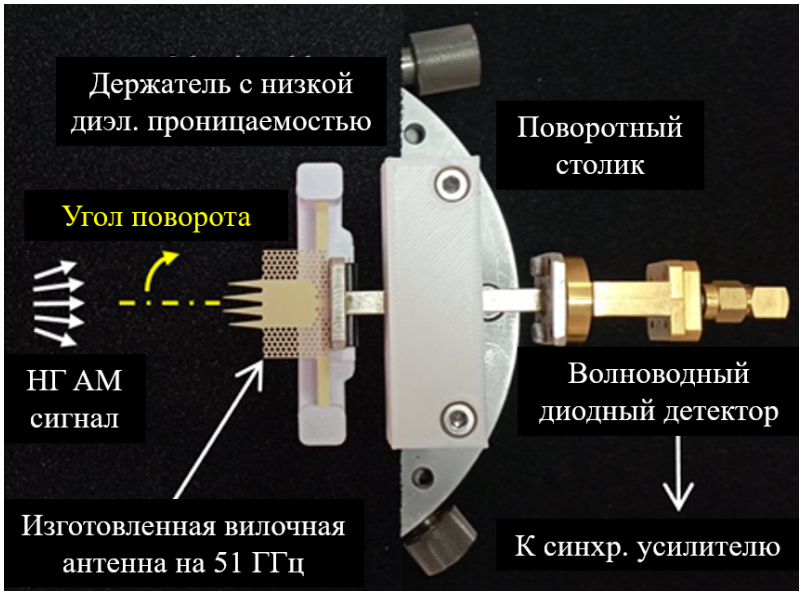

Fig. 4. An experimental installation for measuring the radiation pattern at a frequency of 50-52 GHz.

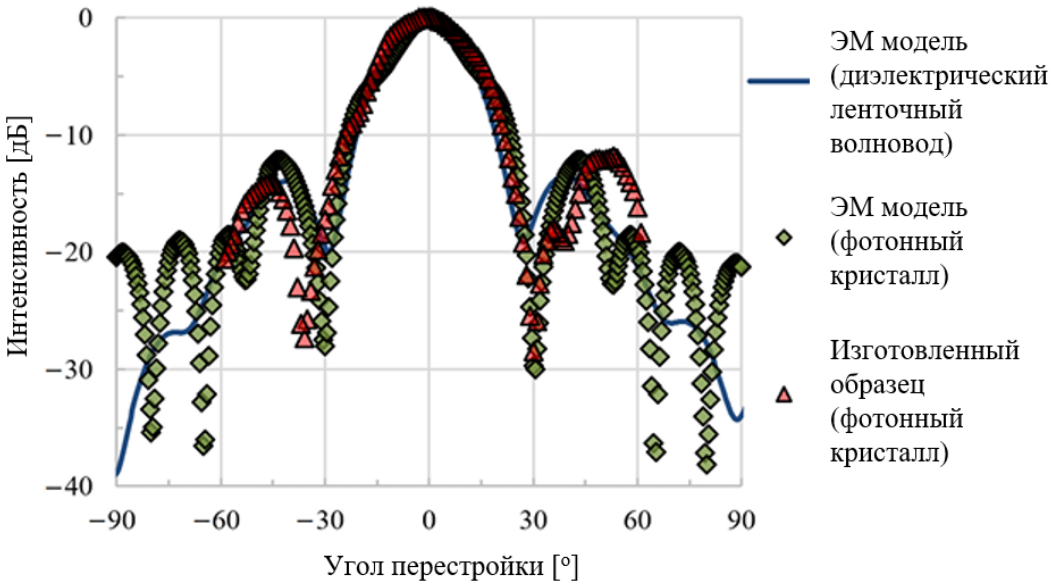

Fig. 5. Directional pattern of a fork dielectric antenna for operation at a frequency of 50-52 GHz.

Figure 4 shows a photograph of an experimental setup for measuring the beam profile, and Figure 5 shows a radiation pattern of a sample in the far field at

a frequency of 51 GHz. The main lobe of the diagram has a width of 27° and is in good agreement with the Gaussian distribution. The level of the side lobes does not exceed -12 dB, which surpasses designs of a similar type presented in the literature [16]. The experimental data obtained confirm the results of EM modeling, according to which the antenna gain should be 11,2 dB with a side lobe level of -12,1 dB and a beam width of 21° for the geometry of the created structure. Similar parameters were obtained for EM models of silicon devices at a frequency of 2,7 THz. A further increase in directivity can be achieved by combining fork antennas into one- or two-dimensional arrays. In our work [A2], the specific propagation losses in dielectric photonic crystal waveguides with a given geometry were also measured. The loss value was less than 0,1 dB/mm. This fact allows us to assert that in the developed silicon designs there should be no additional losses in the input optics (in comparison with the calculation), which significantly affect the sensitivity of the mixer. The details of the waveguide measurements are presented in the text of the dissertation. Based on the results of electromagnetic modeling and verification of the computational model, a silicon-on-insulator (SOI) was chosen as the substrate for the manufacture of samples of HEB mixers with a central operating frequency of 2,7 THz. An image from the SEM for one of the 5 samples of HEB mixers is shown in the figure 6. The mixer is made on the basis of an ultra-thin NbN film (with a layer thickness of ≈4 nm). The sensor element of the mixer is an NbN microbridge with specified linear dimensions of 0,2-0,6×2 microns (L×W). After manufacturing, direct current measurements of the samples were carried out.

The results of measurements of the temperature dependence of the resistance of the samples showed the preservation of the superconducting properties of NbN based on the results of structuring the film and the SOI wafer. The value of the residual series resistance of the samples was 70-80 Ohm. This high value is due to the long and thin bias contacts. This fact may also indicate that the actual area of the microbridges may be different due to defects (beam drift, secondary electron reflections) obtained during the formation of contacts to the NbN using electron

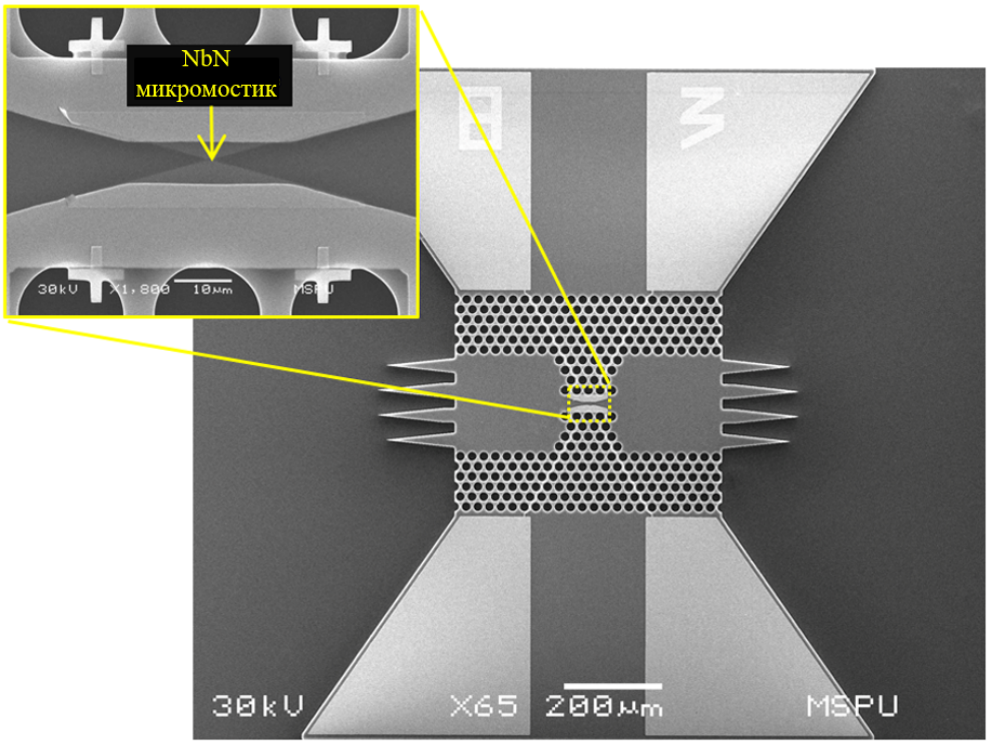

Fig. 6. An image from the SEM of a manufactured sample of a HEB mixer with a central operating frequency of 2.7 THz.

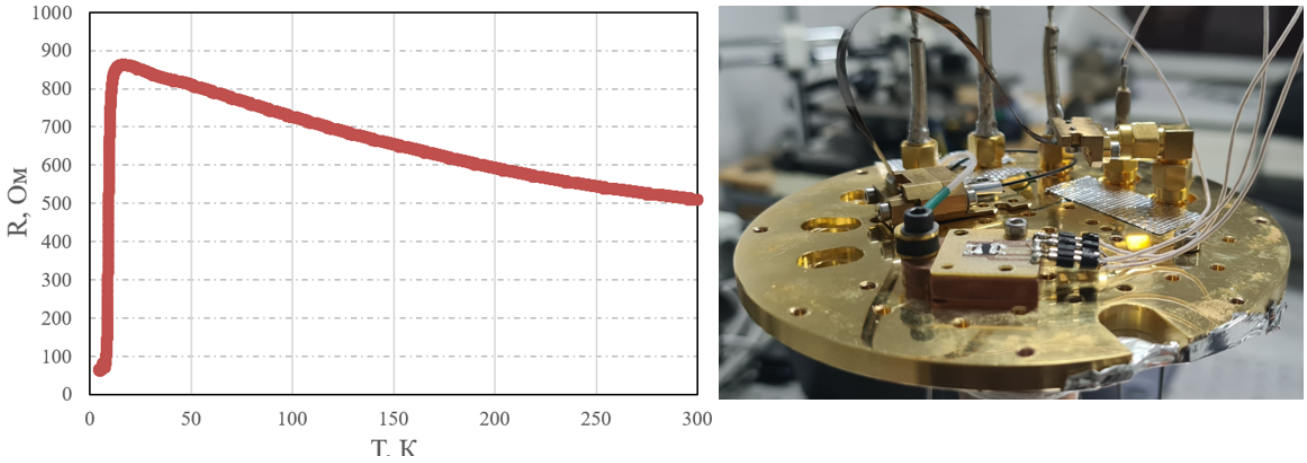

Fig. 7. Measurements of the dependence of resistance on temperature: on the left - experimental data for a sample of a HEB mixer with a central operating frequency of 2,7 THz; on the right - a photograph of the «cold» platform of the 2nd stage of the cryogenic machine with an installed sample.

lithography. The graph also shows that the critical temperature of the sample is 9,3 K with a superconducting junction width of 1,6 K.

The hole diameters of D =18.27±0.47 microns were measured for the manufactured samples of HEB mixers. This average value differs from the set value of D = 18

microns by only 1.5 %. This deviation is most likely caused by a rather thick layer of photoresist formed to protect the sample surface during the BOSCH process. From the point of view of EM wave propagation, the verticality of the created holes is especially important. In the presented sample, the wall angle relative to the substrate plane is 88-89°. The permanent gratings, together with the contours of the power combiner and the photonic crystal waveguide, are almost identical to those specified during the simulation. There were also no deviations in the geometry of the rod antennas after their formation. The calculation and measurement results obtainedas a result of the work make it possible to evaluate the prospects of the proposed designs of HEB devices for an on-chip PIC spectrometer based on a filterbank. Spectrometers with moderate spectral resolution ($F/\Delta F \geq$50) can be used in radio astronomy, since spectral surveys of large areas seem to be significant enough to characterize large-scale astronomical structures and the history of star formation of the Universe using intensity mapping of emission lines.

In the **third chapter** provided original ways to reduce losses in a Ti/Pt/Au/n-GaAs Schottky diode for the frequency range above 100 GHz. The results of experiments on the influence of the layered composition of the planar structure on the transport properties of direct current and alternating current are presented. Calculations and experiments on finding a technological design, selecting processes, and including a diode in a cell of a spatial signal modulator in the 140-150 GHz band are described. The main results were published by the author in [A6—A16].

In the THz range, it becomes necessary to take into account the influence of eddy currents, as well as surface and edge effects on propagation losses in the planar structure of the diode, that limit the sensitivity and performance of planar Schottky diodes. These negative effects depend on the geometry and can be eliminated as soon as the thickness of the GaAs conductive layer matches the thickness of the skin layer at the operating frequency. In case of the planar Schottky diode (PSD) studied in this work, this layer is represented by strongly doped n_+-GaAs (type 1 sample) and a combination of moderately doped n'-GaAs and strongly doped n_+-GaAs (type

2 sample). The difference in doping degrees also causes differences in conductivity. Using the empirical model of mobility in a weak field [17] allows us to calculate the values of the volumetric conductivity of layers at room temperature equal to 433 S/cm for n′-GaAs and 1460 S/cm for n_+-GaAs, which corresponds to the thickness of the skin layer (σ) 3,6 and 2 microns, respectively, for a frequency of 450 GHz. The figure 8 shows the current density distribution in the PSD layer structures calculated using HFSS. It can be seen from the results, that the design of the type 1 planar structure is more technologically advanced and allows the production of thicker mesas with a given contribution of losses caused by geometry through eddy currents.

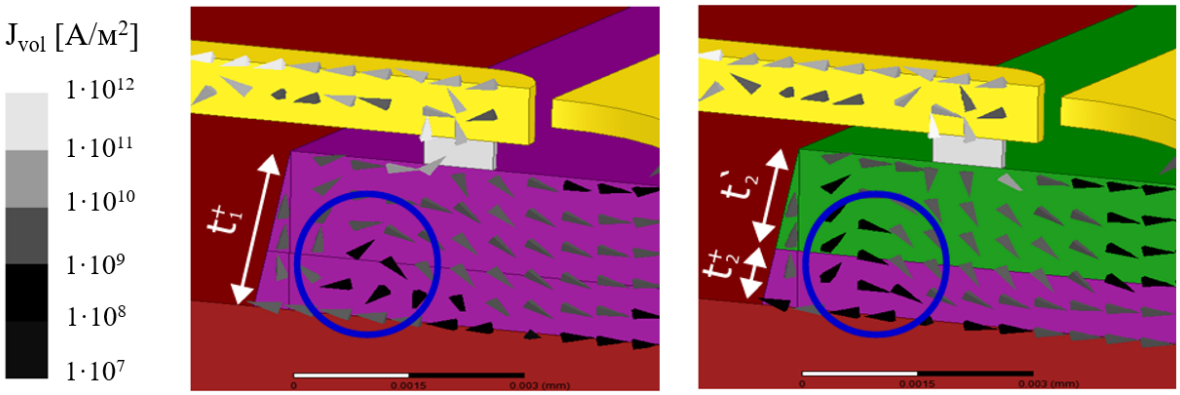

Fig. 8. The distribution of current density in the layered structures of the PSD at a frequency of 450 GHz. On the left: type 1 structure; on the right: type 2 structure.

From the point of view of minimizing losses in the area of the bias lines (anode and cathode electrodes), the creation of ohmic contact to the semiconductor is an important part of the manufacturing technology. The conductive properties of the contact strongly affect the overall performance of the device being manufactured. Multilayer Ni/Au/Ge/Ni/Au (5/45/20/5/100 nm) metallization, which is formed on the surface of a 2 micron thick GaAs layer doped with silicon, was chosen as the ohmic contact system under study. In accordance with the measurement methodology using the modified transmission line method, a series of experiments were conducted on sequential measurement of resistance values ($R_{i,i+1}$) between a pair of adjacent contacts. The measurements were carried out using a standard four-

probe method to exclude the influence of wire resistance and probe-sample contact resistance. The obtained resistance values increase linearly with increasing distance between a pair of ohmic contacts. Assuming the resistances of the n_+-GaAs layer (R_{sh}) are the same over the entire transmission line space, the resistance can be expressed as:

$$R_{i,i+1} = R_{sh}{\omega_c}^{-1}(l_{i,i+1} + 2l_t). \tag{2}$$

Here ω_c is the width of the ohmic contact, $l_{i,i+1}$ is the distance between i pair of transmission line contacts, l_t is the length of the leakage area under the contact. The inclination of the straight line given by the equation 2 allows to get the value of R_{sh} with a known value of ω_c. The value of l_t is located as the intersection point of the extrapolated line $R_{i,i+1}(l_{i,i+1})$ with the axis of the abscissa. The value corresponding to the intersection point must be multiplied by -0,5. The experiment showed a change in l_t from 52,8 to 1,5 microns in response to a change in temperature of T_{RTA} from 300 to 400 °C. At the same time, no significant differences were observed for samples subjected to rapid thermal annealing at temperatures of 400 and 450 °C. The specific contact resistances (ρ_c) were calculated using the equation 3 for «cold» and «hot» samples, which were 2,7 and 0,15 μOhm·cm^2, respectively.

$$\rho_c = R_{sh}{l_t}^2 \tag{3}$$

Thus, a significantly lower contact resistance was obtained compared to the examples presented in the literature for standard AuGe/Ni/Au to n_+-GaAs [18] ohmic contacts.

The prospects of practical application of the proposed methods for reducing losses in a diode have been tested experimentally. To solve this problem, PSD samples were produced using two types of silicon-doped GaAs grown using the method of molecular beam epitaxy (MBE). Detailed information on the layered composition of the grown MBE samples is presented in the table 3.

Table 3. The layered structure of GaAs samples grown by the MBE method. Here t is the thickness, and N is the doping level.

$x^* = 0,8 \pm 0,04$

Structure type	№	Description	t, μm	N, cm^{-3}
1	4	n-GaAs	0,2	4×10^{17}
	3	n_+-GaAs	1,2	5×10^{18}
	2	$Al_xGa_{1-x}As^*$	0,05	–
	1	GaAs layer	0,03	–
	0	i-GaAs(100) wafer	350	–
2	5	n-GaAs	0,15	4×10^{17}
	4	n'-GaAs	0,06	1×10^{18}
	3	n_+-GaAs	0,8	5×10^{18}
	2	$Al_xGa_{1-x}As^*$	0,05	–
	1	GaAs layer	0,03	–
	0	i-GaAs(100) wafer	350	–

On the wafers of both configurations, PSDs with a surface channel were made in spiral antennas, while the manufacturing process route was identical for both types of structures.

The figure 9 shows an SEM photo of a PSD sample, as well as a cross-sectional diagram of the device with an illustration of the layers (the diagram is not scaled).

To carry out experiments with measuring transport properties at direct and alternating currents, a sample of PSD was glued to a hemispherical silicon lens. The lens was mounted in a holder with SMA connectors, which were attached to the arms of the spiral antenna using coaxial-coplanar adapters and conductive paste. The sample holder was connected to an offset adapter, the DC port of which was connected to a measuring source to offset the diode.

The voltage distribution between the spatial charge region and the series resistance in the layered structure of a planar Schottky diode can be expressed using the volt-

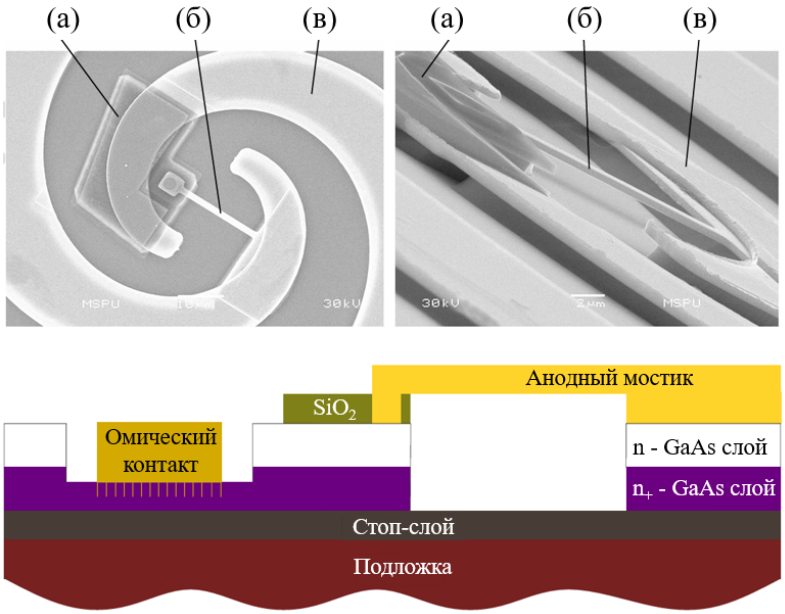

Fig. 9. SEM photos of samples and a diagram of the device. Here а) is an ohmic contact, б) is an anode bridge, and в) is a spiral antenna.

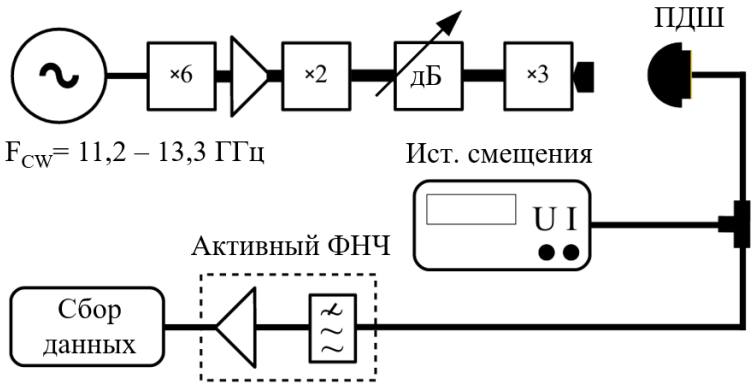

Fig. 10. The scheme of the experimental setup for measuring the characteristics of the PSD.

ampere characteristic (IV) as:

$$I_{re}(V_d) = I_s \left[exp\left(\frac{qV_j(V_d)}{\eta kT} \right) - 1 \right], \tag{4}$$

where $V_j(V_d) = V_d(1 - R_s/R_d(V_d))$. Here V_d is the constant voltage across the diode, R_d is the total resistance of the diode, I_s is the saturation current, q is the electron charge, k is the Boltzmann constant, and T is the physical temperature of the diode. V_j is the voltage drop in the spatial charge region, and R_s is the series resistance. Using R_s as a fitting parameter for the best approximation by the function $I_{re}(V_d)$ and the values of experimentally obtained characteristics of diodes,

the actual value of R_d can be estimated.

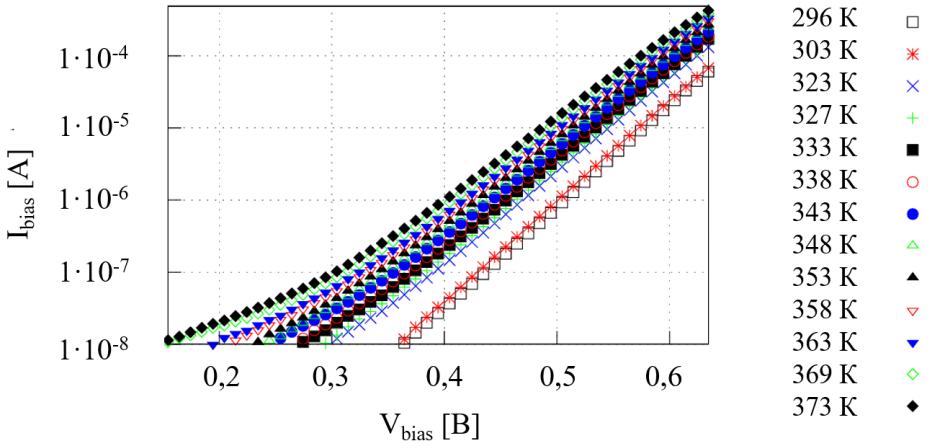

Fig. 11. The group of PSD's IVs for various operating temperatures.

If we assume that the values of the barrier height in the Schottky microcontact area obey the Gauss distribution law, then, according to a study by [19], it is possible to determine the value of the height of the potential barrier at zero displacement current (Φ_{b0}) as:

$$\Phi_{b0} = \Phi_m - {\sigma_s}^2 q(2kT)^{-1}, \tag{5}$$

where Φ_m is the average value of the barrier height, which can be accurately measured using volt-farad characteristic analysis, and σ_s is the standard deviation of the barrier height. The last parameter also depends on temperature, obeying the law ${\sigma_s}^2(T) = {\sigma_s}^2(0) + \alpha_\sigma T$[20]. In addition, it is generally assumed that the height of the potential barrier is essentially the same as the barrier height obtained by analyzing the volt-faraday characteristic [21; 22]. As a result, the equation (5) takes the form:

$$\Phi_{bf} - \Phi_{b0} = {\sigma_s}^2(0) q(2kT)^{-1} + \alpha_\sigma q(2k)^{-1}. \tag{6}$$

Here Φ_{bf} is the height of the potential Schottky barrier, which can be accurately calculated by analysing the volt-farad characteristic. Thus, the uniformity of the Schottky barrier can be determined by comparing the values of Φ_{bf} and Φ_{b0}, the difference of which obeys the inverse dependence on temperature. Dependence analysis

allows you to determine the values of the standard deviation ($\sigma_s(0)$) at zero temperature and the temperature coefficient (α_σ).

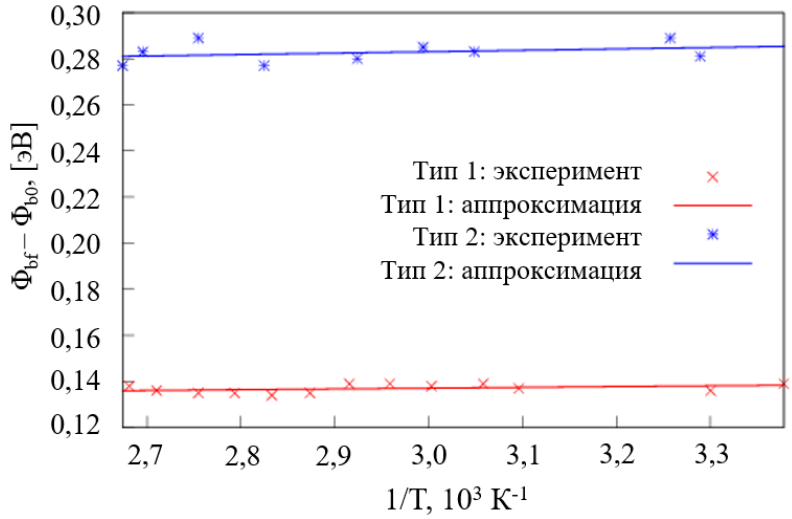

Fig. 12. Temperature dependences of the difference between the barrier height in flat zones and the barrier height at zero displacement current for samples of types 1 and 2.

Figure 12 shows the experimental dependences $\Delta\Phi(T^{-1}) = \Phi_{bf} - \Phi_{b0}$ for samples of type 1 and type 2, equal to $0,0034T^{-1} + 0,127$ and $0,0061T^{-1} + 0,265$, respectively. During the experiment, it was found that the value of the change in the height of the barrier is weakly dependent on temperature. A similar behavior of the temperature dependence was found for the heights of the barriers (Fig. 13), as well as for the ideality factor of the diodes.

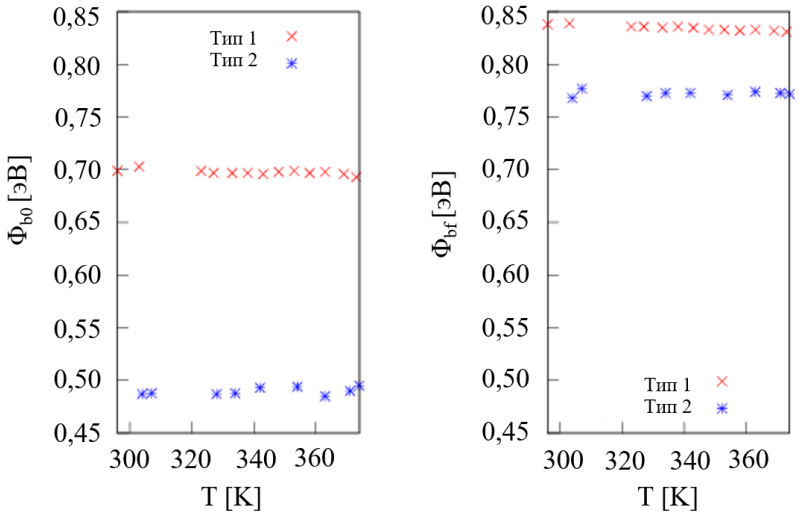

Fig. 13. Temperature dependences of barrier heights for samples of types 1 and 2.

The main parameters, which were evaluated during the IV analysis at room

temperatures, for samples used during AC measurements are shown in the table 4. These measurements were carried out to verify the calculated values of the parasitic parameters of the operating range and to experimentally determine the cut-off frequencies of the operating range.

Table 4. Parameters of the studied quasi-optical samples of PSD.

Samples	D_A, μm	η	R_s, Ohm	Φ_m, eV	σ_s, meV
Type 1	3	1,2	20	0,840	80
Type 2	3	1,5	50	0,762	116

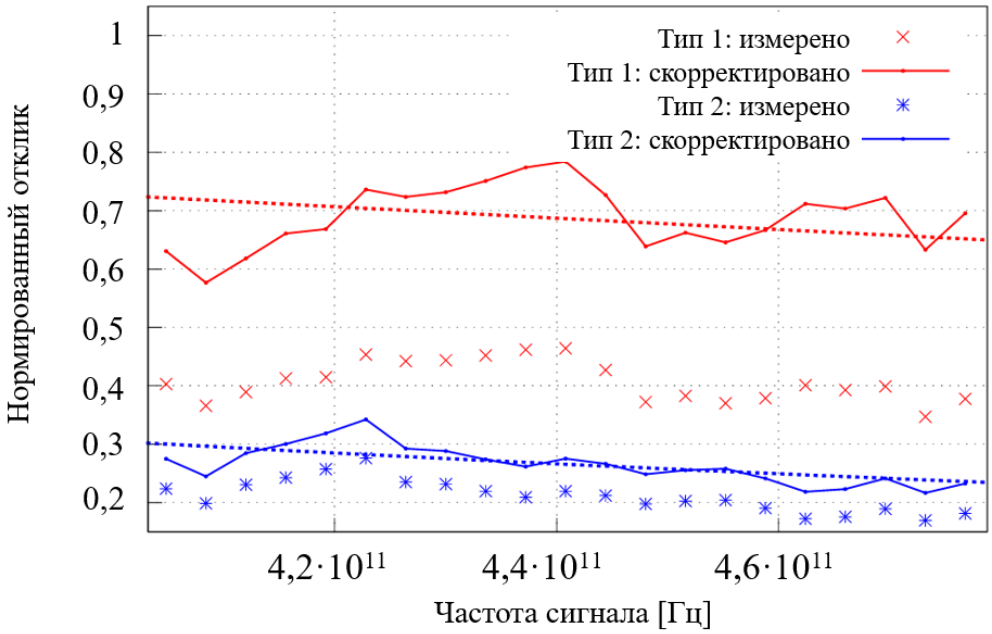

Fig. 14. The response of quasi-optical PSD samples as a function of frequency.

The experimental data were normalized using the function $P_{inc}(f)$ (7) and are approximated by the transmission coefficient of the RC-circuit of the diode, which takes into account the mismatch of the spatial charge region with the input signal due to the frequency-dependent parasitic current through the shunt capacitance.

$$P_{inc}(f) = P_0(1 - |\Gamma|^2), \tag{7}$$

where $P_{inc}(f)$ is the power coming to the internal RC-part of the PSD, P_0 is the power received by the antenna, Γ is the reflection coefficient. A good correspondence

of the approximation curves with the normalized frequency profile of the response voltage of the samples was obtained, which confirms the reliability of the obtained values of the parasitic parameters. Therefore, the cutoff frequency from above (F_c), of the operating range of the remote control with properly selected input optics can be calculated as:

$$F_c = (2\pi R_s C_{tot})^{-1}. \tag{8}$$

Here C_{tot} is the total parasitic capacity of the device. Substituting the corresponding parasitic parameters into the equation (8), we can obtain the cutoff frequencies $F_{c1} = 650$ GHz and $F_{c2} = 265$ GHz for samples of type 1 and 2, respectively. It should be noted that the increased value of the sequential resistance of the type 2 sample is due to the excessive etching of the n_+-GaAs layer during the sample manufacturing process. In addition, Type 2 antenna-free samples demonstrated an R_s value of only 20 Ohm. Thus, it can be concluded that in the general case, the frequency of F_{c2} can be increased to 660 GHz, which means that the samples demonstrate a fairly stable frequency response regardless of the selected GaAs layer structure. Based on the fact that the parasitic capacity is mainly related to the bridge-mesa capacity (C_b), C_{tot} can be significantly reduced by using a thicker layer of SiO_2. At the same time, changes in the thickness of the dielectric layer do not affect the transport parameters of the PSD in any way. If the thickness of the dielectric layer is assumed to be 500 nm, then the calculated values of C_{tot} will be 3,6 fF and 3,4 fF for samples of type 1 and 2, respectively. The cutoff frequency will shift to 2,28 THz.

Based on the results of studies of the etching process, a strong anisotropy of the process was established, which made it possible to propose, design and manufacture a sample of a PSD with an Γ-shaped bridge. Several reasons motivated the development of such a geometry: a) the possibility of forming a diode with a mesa of any given thickness; b) the possibility of creating an integrated device for

radiophysical applications with a Schottky contact of characteristic dimensions of the order of hundreds of nanometers, regardless of the thickness of the GaAs epitaxial layers; c) diodes with reduced parasitic capacitance due to the wide variability of geometric solutions for the Γ-shaped bridge. Due to the established anisotropy of etching for GaAs plates of crystallographic orientation (100), it is possible to obtain a mesa wall with a slope of 45° in two directions relative to the base section of the plate. To create a sample for the experimental verification of the proposed ideas, a plate with the following layered composition was selected: a SI-GaAs substrate with a thickness of 350 microns, an $Al_{0,8}Ga_{0,2}As$ layer with a thickness of 50 nm, epitaxial layers of n_+-GaAs with a thickness of 1,2 microns with a carrier concentration 5×10^{18} cm^{-3} and n-GaAs with a thickness of 0,2 microns and a carrier concentration of 4×10^{17} cm^{-3}. The technological processes have undergone some changes compared to the basic route:

(I) Formation of Ti/Pt/Au Schottky contacts (50/20/20 nm) The creation of a Schottky barrier at the very beginning of the manufacturing process route will allow obtaining a better metal-semiconductor transition boundary, due to less impact on the contact area during technological operations. Metallization was also modified by adding a Pt layer (the essence of the improvement is discussed in detail in [23]) to prevent metal diffusion with the semiconductor during the subsequent rapid thermal annealing operation.

(II) Formation of a 250 nm thick SiO_2 mask in the area around the Schottky contact.

(III) Formation of ohmic contacts. After the electron lithography process, the n-GaAs layer was first etched in a window made of a resist that coincided with the window in SiO_2, followed by plating of the ohmic contact Ni/Ge/Au/Ni/Au (5/20/35/15/80 nm). The last process of this stage was rapid thermal annealing at a temperature of 360 °C for 2 minutes.

(IV) Formation of the mesa. A protective mask was formed from AZ1512 resist, followed by GaAs etching across the field to a stop layer of $Al_{0,8}Ga_{0,2}As$.

(V) Forming the anode contact and the Γ-shaped bridge. A sufficiently thick layer of Ti/Au metallization (5/500 nm) is necessary to ensure a high-quality and stable electrical connection in the areas where the anode bridge passes between the lower and upper planes.

(VI) Formation of output contact pads. In this process, the thickness of the metallization must also be made large enough to ensure the connection of the ohmic contact on the upper plane of the topology with the metallization of the output contact on the lower plane of the topology.

(VII) Formation of a protective layer of the resist followed by etching. Etching was performed using an ammonia etcher H_2O:H_2O_2:NH_3(35%), which made it possible to maintain the smoothness of the surface. The final result is shown in the figure 15.

Using the previously described methods of IV analysis, the characteristics of the PSD were obtained (Fig. 16).

For the best samples, the value of the series resistance was 4 Ohm, and the value of the linearity was 1,2. The capacitance value calculated using EM modeling for the resulting PSD structure was 3 fF. According to the equation 8, for manufactured diodes with the above parameters, the cutoff frequency should be 13 THz. However, taking into account the empirical correction $\times 0,1$ typical for the THz community, we can conclude that the expected range of operating frequencies of diodes in a real system is limited from above to about 1-2 THz. At the same time, radiophotonic and photonic integrated circuits of a lower frequency range of 0,1–0,3 THz using diode technologies are in demand in spatial signal modulators in modern imaging and wireless communication systems.

As part of the preparation of the study, the prospects of using a remote

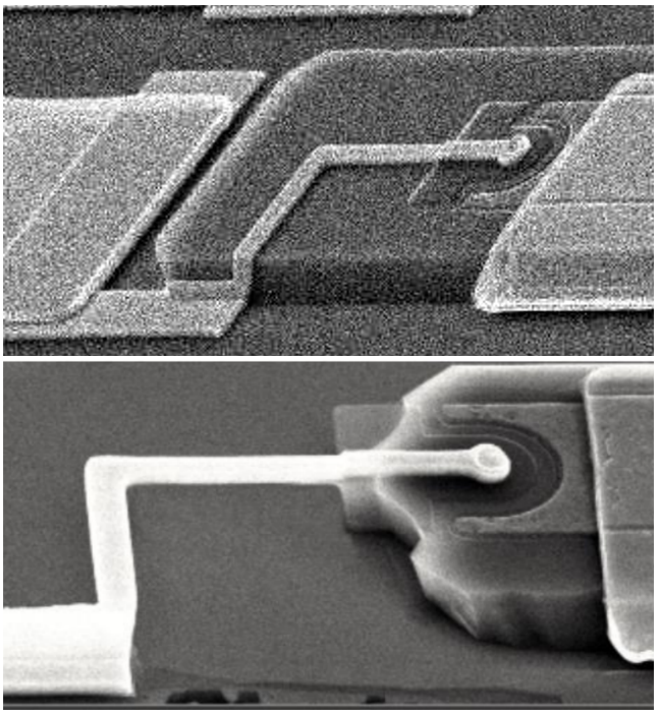

Fig. 15. SEM photos of diode devices with Γ-shaped bridges. Above: a photograph of the structure before the final etching process; below: a photograph of the structure after the etching process.

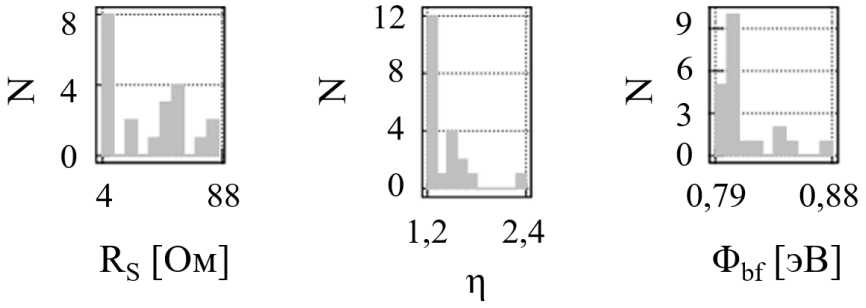

Fig. 16. Characteristics of manufactured diode devices with Γ-shaped bridges.

sensing element as part of a spatial signal modulator cell in the 110-170 GHz band were studied. The radiophysical properties of the cell in terms of the implemented amplitude and phase manipulations were characterized using numerical calculations and prototyping.

In **Conclusion**, the main results obtained as a outcome of the dissertation research are presented.

List of author's publications

A1. Superconducting Electronic–Photonic Platform for HEB-Based Terahertz Spectrometers / A. Shurakov, **I. Belikov**, A. Prikhodko, M. Ershova, G. Goltsman // Applied Sciences. — 2023. — Т. 13, № 10. — С. 5892.

A2. Millimeter wave photonic crystal waveguides fabricated via direct machining / A. Prikhodko, **I. Belikov**, A. Lvov, A. Shurakov, G. Goltsman // St. Petersburg State Polytechnical University Journal: Physics and Mathematics. — 2022. — Т. 15, S3.3. — С. 345—349.

A3. Reflectarray-Assisted Spacial Binning in HEB-Based Terahertz Dispersive Spectrometer / A. Shurakov, A. Lvov, **I. Belikov**, A. Razakova, A. Prikhodko, G. Gol'tsman // 2024 IEEE 9th All-Russian Microwave Conference (RMC). — IEEE. 2024. — С. 196—199.

A4. Terahertz Hot Electron Bolometer Coherent and Direct Detectors Utilizing Si Waveguiding Structures / A. Shurakov, A. Prikhodko, **I. Belikov**, G. Gol'tsman // 2022 IEEE 8th All-Russian Microwave Conference (RMC). — IEEE. 2022. — С. 19—22.

A5. Terahertz HEB-based on-chip spectrometers for material and biomedical studies / A. Shurakov, A. Prikhodko, **I. Belikov**, G. Goltsman // Сборник трудов конференции «International Conference on Advanced Laser Technologies (ALT)». — Федеральное государственное бюджетное учреждение науки Федеральный ... 2023. — С. 236—236.

A6. Ti/Au/n-GaAs planar Schottky diode with a moderately Si-doped matching sublayer / A. Shurakov, P. Mikhalev, D. Mikhailov, V. Mityashkin, I. Tretyakov, A. Kardakova, **I. Belikov**, N. Kaurova, B. Voronov, I. Vasil'evskii [и др.] // Microelectronic Engineering. — 2018. — Т. 195. — С. 26—31.

A7. Empirical blockage characterization and detection in indoor sub-THz communications / A. Shurakov, D. Moltchanov, A. Prikhodko, A. Khakimov, E.

Mokrov, V. Begishev, **I. Belikov**, Y. Koucheryavy, G. Gol'tsman // Computer Communications. — 2023. — Т. 201. — С. 48—58.

A8. Planar Schottky diode with a Γ-shaped anode suspended bridge / A. Shurakov, D. Mikhailov, **I. Belikov**, N. Kaurova, T. Zilberley, A. Prikhodko, B. Voronov, I. Vasil'evskii, G. Goltsman // Journal of Physics: Conference Series. Т. 1695. — IOP Publishing. 2020. — С. 012154.

A9. Integrated Circuit of an Intelligent Reflecting Surface for sub-THz Wireless Communication / A. Shurakov, A. Prikhodko, **I. Belikov**, A. Razakova, G. Gol'Tsman // 2023 IEEE 18th International Conference on Nano/Micro Engineered and Molecular Systems (NEMS). — IEEE. 2023. — С. 183—187.

A10. Wafer-thick GaAs Photonic-electronic Platform for Fast Terahertz Beam Steerers / A. Shurakov, A. Prikhodko, **I. Belikov**, G. Gol'Tsman // 2024 Photonics & Electromagnetics Research Symposium (PIERS). — IEEE. 2024. — С. 1—5.

A11. Towards multipixel THz Schottky diode detector with a single RF output line / A. Prikhodko, **I. Belikov**, D. Mikhailov, A. Shurakov, G. Goltsman // Journal of Physics: Conference Series. Т. 2086. — IOP Publishing. 2021. — С. 012063.

A12. Efficiency of a microwave reflectometry for readout of a THz multipixel Schottky diode direct detector / A. Shurakov, A. Prikhodko, D. Mikhailov, **I. Belikov**, N. Kaurova, B. Voronov, G. Goltsman // Journal of Physics: Conference Series. Т. 1695. — IOP Publishing. 2020. — С. 012156.

A13. Ultra-deep wet chemical etching of GaAs upon fabrication of mmwave sensors / **I. Belikov**, A. Shurakov, A. Prikhodko, G. Gol'tsman // The 5-th lnternational Conference «Terahertz and Microwave Radiation: Generation, Detection and Applications»
(TERA-2023). — 2023. — С. 82—82.

A14. Nondestructive KPFM-assisted Quality Control in Fabrication of GaAs High-Speed Electronics / A. Shurakov, N. Kaurova, **I. Belikov**, T. Zilberley, A. Prikhodko, B. Voronov, G. Gol'tsman // arXiv preprint arXiv:2212.01474. — 2022.

A15. Membrane-integrated planar Schottky diodes for waveguide mm-wave detectors / A. Shurakov, **I. Belikov**, A. Prikhodko, D. Mikhailov, G. Gol'tsman // Microwave and Telecommunication Technology. — 2021. — Т. 3. — С. 34.

A16. *Патент на полезную модель*. Конструкция интеллектуальной отражающей поверхности на основе фотонного кристалла арсенида галлия / Ш. А.С. ; Ф. государственное бюджетное образовательное учреждение высшего образования "Московский педагогический государственный университет" (МПГУ). — № RU233164U1 ; заявл. 26.06.2024 ; опубл. 08.04.2025, Бюл. № 10. — 5 с. : 2 ил.

A17. Terahertz detector utilizing a SiO2/Graphene/SiO2 sandwich suspended at the feed of a planar antenna / **I. Belikov**, M. Rybin, A. Prikhodko, D. Mikhailov, I. Gayduchenko, A. Shurakov, G. Goltsman // Journal of Physics: Conference Series. Т. 2086. — IOP Publishing. 2021. — С. 012048.

References

1. *Withayachumnankul W.* [и др.]. Integrated silicon photonic crystals toward terahertz communications // Advanced Optical Materials. — 2018. — Т. 6, № 16. — С. 1800401.
2. Terahertz topological photonic integrated circuits for 6G and beyond: A Perspective / A. Kumar [и др.] // Journal of Applied Physics. — 2022. — Т. 132, № 14.
3. *Koala R. A.* [и др.]. Nanophotonics-inspired all-silicon waveguide platforms for terahertz integrated systems // Nanophotonics. — 2022. — Т. 11, № 9. — С. 1741—1759.
4. *Sengupta K.* [и др.]. Terahertz integrated electronic and hybrid electronic–photonic systems // Nature Electronics. — 2018. — Т. 1, № 12. — С. 622—635.
5. *Shurakov A.* [и др.]. Superconducting hot-electron bolometer: from the discovery of hot-electron phenomena to practical applications // Superconductor Science and Technology. — 2015. — Т. 29, № 2. — С. 023001.
6. A D-band joint radar-communication CMOS transceiver / W. Deng [и др.] // IEEE Journal of Solid-State Circuits. — 2022. — Т. 58, № 2. — С. 411—427.
7. *Fujishima M.* Overview of sub-terahertz communication and 300GHz CMOS transceivers // IEICE Electronics Express. — 2021. — Т. 18, № 8. — С. 20212002—20212002.
8. Arsenides-and related III-V materials-based multilayered structures for terahertz applications: Various designs and growth technology / A. E. Yachmenev [и др.] // Progress in Crystal Growth and Characterization of Materials. — 2020. — Т. 66, № 2. — С. 100485.

9. InP/CMOS co-integration for energy efficient sub-THz communication systems / C. Desset [и др.] // 2021 IEEE Globecom Workshops (GC Wkshps). — IEEE. 2021. — С. 1—6.

10. Wireless communications through reconfigurable intelligent surfaces / E. Basar [и др.] // IEEE access. — 2019. — Т. 7. — С. 116753—116773.

11. Reconfigurable intelligent surface-based wireless communications: Antenna design, prototyping, and experimental results / L. Dai [и др.] // IEEE access. — 2020. — Т. 8. — С. 45913—45923.

12. Active metasurface for reconfigurable reflectors / B. Ratni [и др.] // Applied Physics A. — 2018. — Т. 124. — С. 1—8.

13. A Promising Technology for 6G Wireless Networks: Intelligent Reflecting Surface / W. Long [и др.] // Journal of Communications and Information Networks. — 2021. — Т. 6, № 1. — С. 1—16.

14. Design of a broadband single-layer linearly polarized reflectarray using four-arm spiral elements / F. Xue [и др.] // IEEE Antennas and wireless propagation letters. — 2016. — Т. 16. — С. 696—699.

15. *Yang F.* [и др.]. Terahertz reconfigurable intelligent surfaces (RISs) for 6G communication links // Micromachines. — 2022. — Т. 13, № 2. — С. 285.

16. Fully dielectric rod antenna arrays with integrated power divider / H. Tesmer [и др.] // Frequenz. — 2019. — Т. 73, № 11/12. — С. 367—377.

17. *Sotoodeh M.* [и др.]. Empirical low-field mobility model for III–V compounds applicable in device simulation codes // Journal of applied physics. — 2000. — Т. 87, № 6. — С. 2890—2900.

18. Ohmic contacts for room-temperature AlGaAs/GaAs quantum cascade lasers (QCL) / A. Baranska [и др.] // Optica Applicata. — 2013. — Т. 43, № 1.

19. *Werner J. H.* [и др.]. Barrier inhomogeneities at Schottky contacts // Journal of applied physics. — 1991. — Т. 69, № 3. — С. 1522—1533.

20. *Werner J. H.* [и др.]. Temperature dependence of Schottky barrier heights on silicon // Journal of applied physics. — 1993. — Т. 73, № 3. — С. 1315—1319.

21. *Hübers H.-W.* [и др.]. Temperature dependence of the barrier height of Pt/n-GaAs Schottky diodes // Journal of applied physics. — 1998. — Т. 84, № 9. — С. 5326—5330.

22. Analysis of Electrical Properties of Ti/Pt/Au Schottky Contacts on (n)GaAs Formed by Electron Beam Deposition and RF Sputtering / B. Sehgal [и др.]. — 2003. — Янв.

23. Long-term reliability of Ti–Pt–Au metallization system for Schottky contact and first-level metallization on SiC MESFET / A. Sozza [и др.] // Microelectronics reliability. — 2004. — Т. 44, № 7. — С. 1109—1113.

24. Unit cell model of a terahertz intelligent reflecting surface with Schottky microcontacts / A. Prikhodko [и др.] // Proceedings of the 35th European Modeling and Simulation Symposium (EMSS 2023). Т. 19. — 2023.